Nuclear Engineering and Technology 54 (2022) 234–243

Contents lists available at ScienceDirect

Nuclear Engineering and Technology

journal homepage: www.elsevier.com/locate/net

Original article

Structural and radiological characterization of irradiated RBMK-1500 reactor graphite

Elena Lagzdina [a, *], Danielius Lingis [a], Artūras Plukis [a], Rita Plukienė [a], Darius Germanas [a], Andrius Garbaras [a], Jevgenij Garankin [a], Arūnas Gudelis [b], Ilja Ignatjev [c], Gediminas Niaura [c], Sergej Krutovcov [d], Vidmantas Remeikis [a]

[a] Department of Nuclear Research, Center for Physical Sciences and Technology, Savanorių Ave. 231, LT-2300 Vilnius, Lithuania
[b] Department of Metrology, Center for Physical Sciences and Technology, Savanorių Ave. 231, LT-02300 Vilnius, Lithuania
[c] Department of Organic Chemistry, Center for Physical Sciences and Technology, Saulėtekio Ave. 3, LT-10257 Vilnius, Lithuania
[d] State Enterprise Ignalina Nuclear Power Plant, Elektrinės str. 4, Drūkšinių vil, LT-31152, Visaginas mun, Lithuania

ARTICLE INFO

Article history:
Received 24 December 2020
Received in revised form
4 June 2021
Accepted 25 July 2021
Available online 26 July 2021

Keywords:
RBMK nuclear graphite
Raman spectroscopy
MCNP
Displacements per atom (DPA)
^{14}C

ABSTRACT

This study aims to characterize the irradiated RBMK-1500 nuclear graphite in terms of both structural and radiological properties. The experimental results of morphological and structural analysis of the irradiated graphite samples by using SEM, Raman spectroscopy as well as the theoretical evaluation of primary displacement damage are presented. Moreover, the experimental and theoretical evaluation of the neutron flux is provided and the presence of several γ emitters in the analyzed graphite samples is assessed. Furthermore, the improved version of rapid analysis method for ^{14}C activity determination is applied and the experimentally obtained results are compared with calculated ones. Results indicate that structural changes are uniform enough in all the analyzed samples. However, the distribution of radionuclides is non-homogeneous in the irradiated RBMK-1500 reactor graphite matrix. The comprehensive understanding of both structural and radiological characteristics of nuclear graphite is very important when dealing with decision about irradiated graphite waste management strategy or treatment options prior to its final disposal.

1. Introduction

Ignalina Nuclear Power Plant (INPP) in Lithuania consists of two units of RBMK-1500 (Russian: РБМК, Реактор Большой Мощности Канальный (High Power Channel-type Reactor)) water-cooled graphite-moderated channel-type power reactor. INPP Unit 1 was shut down at the end of 2004, while Unit 2 at the end of 2009. The decommissioning process is in progress for more than ten years and it requires the strategy how to handle the irradiated graphite waste. The total mass of irradiated graphite at INPP is about 3820 tons [1].

The main structural component of the RBMK-1500 reactor core is the cylindrical graphite stack. The main function of the graphite stack of the RBMK-1500 reactor is neutron moderation and reflection, but it also provides structural integrity as well as relatively large heat capacity in case a temporary cooling malfunction occurs [2]. The stack is assembled from various GR-280 grade graphite blocks stacked into columns. The axial openings in the middle of each column serve as fuel channels (FC) or the special purpose channels (e.g., control and protection system (CPS) channels, radial reflector cooling (RRC) channels). FC and CPS channels within the RBMK-1500 reactor core are positioned by using special rings and sleeves, which both are made of GRP-2-125 grade graphite [3]. During reactor operation process these rings provide heat transfer from the graphite stack to the coolant which flows over the channel. Moreover, they serve as compensators in case the channels and graphite blocks change in dimensions due to the heat and radiation [4]. The graphite blocks located within the radial reflector are filled by graphite rods manufactured from GRP-1-280 grade graphite. These graphite rods join the blocks within the column increasing the density and neutron reflecting effectiveness [3].

Graphite as a major structural component material of the RBMK-1500 nuclear reactor core is subjected to high levels of radiation, which leads to changes in both physical and chemical properties of

* Corresponding author.
E-mail address: elena.lagzdina@ftmc.lt (E. Lagzdina).

https://doi.org/10.1016/j.net.2021.07.039

the material. The neutrons produced by nuclear fission fall in a wide range of energy – from an eV to ~10 MeV, with a mean energy of about 2 MeV. These high energy neutrons are scattered by carbon atoms in the graphite matrix either elastically or inelastically. The binding energy of the carbon atom in the graphite crystal lattice is ~7 eV, thus the kinetic energy transferred from the colliding neutron displace the carbon atom from its original lattice site. Displacements are produced by neutrons with energies greater than ~100 eV [5]. The displaced atoms lead to cascade damage events, they also can move in the graphite matrix between layers losing their energy without displacing atoms and finally aggregate in form of the defect clusters. To quantify the primary displacement damage DPA (displacement per atom) units are used. DPA refers to the average number of times an atom is displaced from its original lattice site. Evaluation of the primary displacement damage in the neutron irradiated RBMK-1500 graphite was performed recently [6].

Since the nuclear reactor operates under high temperature conditions the dynamical mechanisms of the defect creation and recombination are accelerated by the thermal effects. In case of RBMK type reactor the maximum calculated graphite temperature is 750 °C, however, the average temperature of the graphite stack during operation is about 500 °C [2,7]. The displacement damage results in creation of in interstitial-vacancy pairs (also known as Frenkel pairs). The formation of these defects and their mobility is temperature dependent [8]. In this work the nature of defects in the irradiated RBMK-1500 reactor graphite matrix is characterized by using scanning electron microscopy (SEM) and Raman spectroscopy techniques.

Intensive neutron flux in the nuclear reactor core leads not only to the structural changes in the graphite matrix but also to accumulation of radionuclides which are produced due to the activation process. ^{14}C is one of the limiting radionuclides in case of disposal of irradiated graphite waste not only from RBMK type reactors, but also from other nuclear reactors, such as UNGG, Magnox, etc [9–11]. There are three reactions involved in ^{14}C production in the graphite matrix under reactor operational conditions: $^{14}N(n,p)^{14}C$, $^{13}C(n,\gamma)^{14}C$ or $^{17}O(n,\alpha)^{14}C$. However, the impact of each mechanism strongly depends on the both isotopic abundance and neutron capture cross section of the precursor. Thus, the ^{14}C production from ^{17}O is not significant due to the low both isotopic abundance as well as neutron capture cross section (0.24 b). The neutron capture cross section of ^{13}C is also very low (0.0014 b). However, ^{13}C is a stable minor isotope of carbon with isotopic abundance of 1.07%, so it is naturally present and homogeneously distributed in the graphite matrix. The neutron capture cross section of ^{14}N is 1.83 b. ^{14}N is found in graphite matrix in the form of impurity, where it is non-homogeneously distributed during manufacturing process and/or randomly absorbed from the atmosphere on the surface of pores located near the surface. Furthermore, in the RBMK-1500 reactor the gas mixture (the standard composition is 10 % nitrogen and 90 % helium, by volume) is supplied through the gaps between the tubes and blocks at a pressure of 0.49–1.96 kPa during the operation time [2]. This may serve as an additional source of ^{14}N for ^{14}C production. The ^{14}C specific activity in the irradiated RBMK-1500 reactor graphite is about 10^5 Bq/g in the reactor core, while up to one order of magnitude lower in the graphite reflectors [12,13]. The presence of other impurities leads to production of different long-lived radionuclides, so they are also investigated [14].

The evaluation of both structural and radiological properties of irradiated graphite is very important for optimization of decommissioning process of RBMK-1500 reactor. Based on this knowledge, the behavior of irradiated graphite as nuclear waste may be revealed and the best way of treatment and/or disposal may be proposed. The structural analysis of irradiated graphite from INPP was not performed before, so the aim of this work is to provide morphological and radiological characterization of irradiated RBMK-1500 nuclear graphite.

2. Materials and methods

2.1. Sample preparation

Graphite samples were obtained from the INPP RBMK-1500 reactor, in which graphite was used as both a moderator and a reflector. Sample ***No.1*** was selected from the central zone, where it was located near the temperature channel. The samples ***No.2–4*** were taken from the central plateau zone of the RBMK-1500 reactor core, while the sample ***No.5*** was from the peripheral zone (See Fig. 1 and Fig. 2).

At first the structural analysis and γ measurements were performed by using the bulk samples, then the certain parts of initial samples were prepared for both stable carbon isotope ratio ($\delta^{13}C$) and ^{14}C measurements. The samples used for stable carbon isotope ratio ($\delta^{13}C$) measurements are noted as ***No.1a***, ***No.2a***, etc., while ones used for ^{14}C analysis as ***No.1b***, ***No.2b***, etc.

2.2. Scanning electron microscopy (SEM)

The scanning electron microscopy (SEM) was employed to examine the microstructure of the graphite samples. The high-resolution images of the reactor irradiated graphite sample ***No.1*** form the central zone and sample ***No.5*** from the peripheral zone as well as raw graphite sample surface were obtained by using SEM Helios NanoLab 650 equipment. An accelerating voltage of 3 kV and an electron beam current of 0.80 nA was used to acquire the electron micrographs of the examined area of the sample.

2.3. Raman spectroscopy

The graphite samples were characterized by Raman spectroscopy at ambient conditions using a Renishaw inVia spectrometer. The samples were placed under a Leica microscope with the 50 × objective lens and 0.75 numerical aperture (NA). Samples were excited with 532 nm continuous wave laser radiation. The 1800 grooves/mm grating was used. Laser power at the sample was restricted to 0.3 mW to avoid the heating effect. Spectra were acquired from 3–5 areas of each sample, while each individual spectrum was collected over 100 s. All spectra were registered in

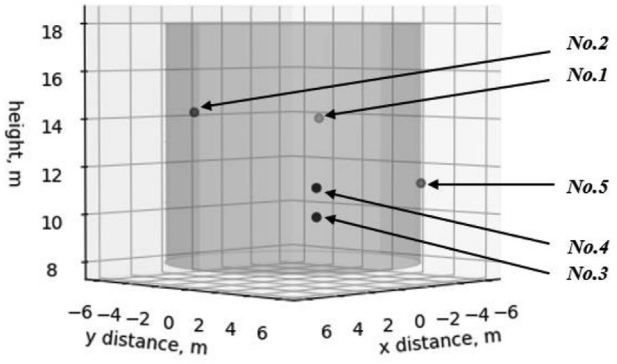

Fig. 1. The positions of the samples in the RBMK-1500 reactor core. Sample ***No.1*** was selected from the central zone, the samples ***No.2–4*** were taken from the central plateau zone of the RBMK-1500 reactor core. Samples ***No.3*** and ***No.4*** were taken from the same channel, but different height. Sample ***No.5*** was from the peripheral zone.

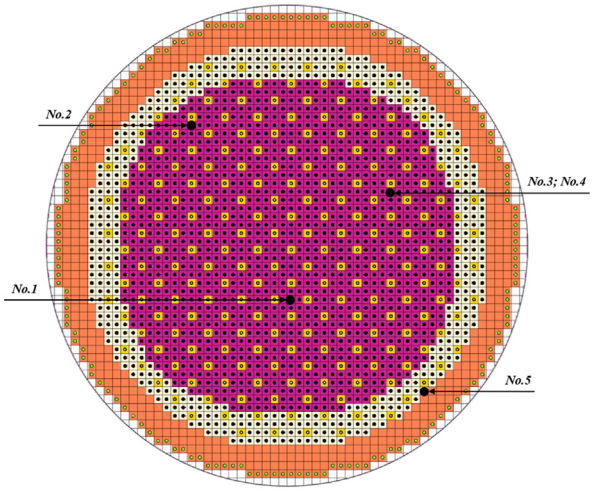

Fig. 2. The cross section of the full scale MCNP6 3D model of the RBMK-1500 reactor core and sample positions.

the Raman shift range from 1000 to 3000 cm^{-1}. Before and after the measurements, a silicon sample spectrum was acquired and a 520.7 cm^{-1} peak was used for the wavenumber axis calibration.

2.4. Evaluation of primary displacement damage

Neutron induced primary displacement damage evaluations were performed based on the neutron flux distribution from the MCNP reactor core model and nuclear data library processing code NJOY2016 [15], with additional evaluation based on SPECTRA-PKA [16]. NJOY2016 is a widely used tool for processing ENDF-6 format [17] files based on users instructions [18]. The code consists of main modules, each having a well-defined processing function. Cross sections were obtained from ^{12}C and ^{13}C ENDF/B-VIII.0 nuclear data libraries, reconstructed at 600 K temperature. In this research the evaluation of displacement damage was based on HEATR and GROUPR modules. HEATR module generates point-wise displacement damage energy and heat production cross sections. The total displacement damage energy production cross section (eV-barn) is obtained by evaluating MT = 444, which covers elastic, inelastic and neutron disappearance processes. The total damage energy is then obtained by combining the cross section with the corresponding flux. The damage energy is modified by Robinson partition function (see [19]) and the number of displaced atoms is evaluated based on NRT (Norgett, Robinson, Torrens) method [19]:

$$DPA = (0.8 \times T)/(2 \times E_d) \quad (1)$$

here T is the total damage energy, E_d is the threshold energy to create a displacement. In this research the threshold energy for all approaches was set to 28 eV.

Another approach to evaluate the displacement damage was based on GROUPR module and SPECTRA-PKA code. The GROUPR module of NJOY evaluates group-to-group recoil cross-section matrices from ENDF-6 files. This way provides possibility to obtain matrices for every available reaction. By combining the recoil matrices with the corresponding neutron flux, one can obtain PKA and particle production spectra. For this, SPECTRA-PKA code was used. It is a command-line driven program for estimation of PKA spectra for a given target nuclide under neutron irradiation. To evaluate the displacements, the code requires recoil matrices, neutron flux, and user input files. The authors of the code provide prebuilt neutron induced PKA production matrices based on TENDL2015 nuclear data. However, in this research we also used reaction matrices based on ENDF/B-VIII.0 nuclear data library obtained with GROUPR module. The combination of recoil matrices and neutron flux is also modified by Robinson partition function and the number of displacements is obtained based on NRT method.

For comparison reasons, neutron induced primary displacement damage was also evaluated by using GEANT4 [20] approach based on NRT method. The technique was detailed previously [6] and will not be discussed here.

2.5. γ-ray spectrometry

In order to determine the presence of γ-ray emitters as well as their activity in the sample, the γ-spectrometric analysis was carried out. Graphite samples were measured using a γ-ray spectrometer equipped with a HPGe well-type detector with a crystal volume of 170 cm^3 and an energy resolution of 2.05 keV at a full-width at the half peak maximum (FWHM) of 1332.5 keV.

2.6. Stable carbon isotope ratio ($\delta^{13}C$) measurements

In order to estimate the total neutron flux in different parts of RBMK-1500 reactor, the stable carbon isotope ratio ($\delta^{13}C$) in irradiated as well as raw graphite samples was measured. During the sample preparation procedure graphite was mixed with the magnesium perchlorate ($Mg(ClO_4)_2$) as an oxidizing material and placed into a tin capsule. Then the measurements were carried out by using the elemental analyzer FlashEA 1112 (*Thermo Fisher Scientific, USA*) connected to the Thermo Finnigan DeltaPLUS Advantage stable isotope ratio mass spectrometer (*Thermo Fisher Scientific, USA*). More detailed description of experimental setup can be found elsewhere [21].

2.7. Calculation of ^{13}C and ^{14}C production

The production of ^{13}C and ^{14}C in the irradiated graphite of the RBMK-1500 reactor has been obtained by modeling of the 3D reactor core with computer code MCNP6 [22]. It should be noted that full scale MCNP6 3D model of RBMK-1500 core has been developed in earlier studies [23–25] and was adapted for calculation of neutron fluxes and neutron reactions in particular graphite construction. For analysis of the generation of ^{13}C and ^{14}C in the RBMK-1500 reactor core graphite the new nuclear data libraries for ^{12}C and ^{13}C isotopes have been used [26].

The plan view of the full scale MCNP6 3D model of the RBMK-1500 reactor is given in Fig. 2. The full scale MCNP6 3D model is made of 1661 fuel assemblies and 223 control rods (CR) in the graphite matrix with a realistic distribution of the control rods. In this case the configuration with extracted control rods as well as with ^{135}Xe admixture (0.46 ppm) for compensation of the reactivity excess to obtain k_{eff} ~1 (k_{eff} = 1.0201 ± 0.0002) was used. The measured power distribution in the RBMK-1500 reactor is more "flat" compared with the simulated one. However, the power intensity does not vary more than 20 % in both core plateau and periphery zone, while it decreases in the reflector zone [25]. In order to obtain the neutron flux at the particular sample position (both certain region of the reactor core and height), the MCNP6 3D model is adjusted according to the real axial and radial power of the INPP [27]. By using MCNP6 code the $^{14}N(n, p)^{14}C$ and $^{13}C(n, \gamma)^{14}C$ reaction rates in the RBMK-1500 reactor graphite are calculated as follows:

$$RR_i = N \int_0^{\infty} \sigma(E)\phi(r,E)dE \quad (2)$$

here RR_i – is rate at which reactions are occurring in the nuclide i (reactions/s); N - number of target atoms in the sample; $\sigma(E)$ - energy-dependent microscopic cross-section; and $\phi(r,E)$ - energy-dependent neutron flux in the sample (n/cm^{2}s).

2.8. ^{14}C activity determination

To determine ^{14}C activity in the irradiated graphite samples experimentally, the rapid analysis method was applied [12]. Prior to the analysis the graphite samples were weighted by using a XP105 (*Mettler-Toledo, Switzerland*) dual range balance. The obtained results are referred as sample mass by weighing. Then these graphite samples were packed in the 8 × 5 mm pressed tin capsules (*Elemental Microanalysis, UK*) and mixed with magnesium perchlorate (*SÄNTIS Analytical, Switzerland*) as the oxidizing material to enhance the combustion process. Graphite samples were combusted using an elemental analyzer Thermo Flash EA 1112 (*Thermo Fisher, USA*). After the combustion event the CO_2 amount was estimated by using the thermal conductivity detector (TCD). The obtained results are referred as sample mass by CO_2 amount or sample mass by combustion. After TCD the CO_2 gas passed through the custom made tubing system to the β particle registration system and finally to the two CO_2 gas catchers filled with 3 M NaOH solution designed to capture ^{14}C.

^{14}C activity determination was carried out based on the β-particle registration in CO_2 gas flow by using Passivated Implanted Planar Silicon (PIPS) (*Canberra, USA*) semiconductor detectors. The β-particle registration system was incorporated between the sample combustion system and alkaline CO_2 gas catchers. During sample combustion process the CO_2 gas from elemental analyzer system passed through the β-particle detection chamber where two PIPS detectors were located. Pulses from each of the detectors were amplified by using an Ortec 142 (*Ortec, USA*) preamplifier and registered with a DSA1000 (*Canberra, USA*) system as can be seen in Fig. 3.

The β-particle activity spectrum was measured with a time step interval of 60 s, while the total time of sample combustion was preset to 600 s. Finally, each spectrum was integrated to find out the sum of pulses per step.

As the cross-check of the ^{14}C activity determination by semiconductor β-particle detection system, the liquid scintillation counting (LSC) was applied. By using this method the ^{14}C activity in alkaline 3 M NaOH solution catchers was examined. The 4 ml of exposed solution was mixed with 16 ml of liquid scintillation cocktail Opti-Phase HiSafe 3 (*PerkinElmer, USA*) and subsequently measured with a liquid scintillation counter Quantulus-1220 (*PerkinElmer, USA*). Based on the obtained LSC spectrum the ^{14}C activity in the combusted graphite sample was obtained.

Based on the sample mass obtained independently by both weighing and combustion methods and β activity of the sample registered by semiconductor detector as well as LSC method, the specific activity of ^{14}C in the irradiated graphite samples was evaluated. The detailed description of the rapid analysis method for the determination of ^{14}C specific activity in irradiated graphite was published previously [12].

3. Results and discussion

3.1. Structural analysis: SEM and Raman spectroscopy

The structural properties of irradiated RBMK-1500 reactor graphite samples were analyzed experimentally by using scanning electron microscopy (SEM) and Raman spectroscopy techniques. The SEM images of the irradiated graphite samples as well as raw graphite sample are shown in Fig. 4. In general, nuclear graphite exhibits the non-homogenous morphology which is seen in the micrographs of both irradiated and raw graphite samples. However, the damaged structure is especially visible in the micrographs of the sample from the central zone of the reactor. As can be seen from the micrographs, there are a lot of small cracks and pores. The small crystallites are randomly oriented.

The surface of the irradiated RBMK-1500 reactor graphite was also studied by using Raman spectroscopy. This method is widely used to investigate the structural properties of carbonaceous

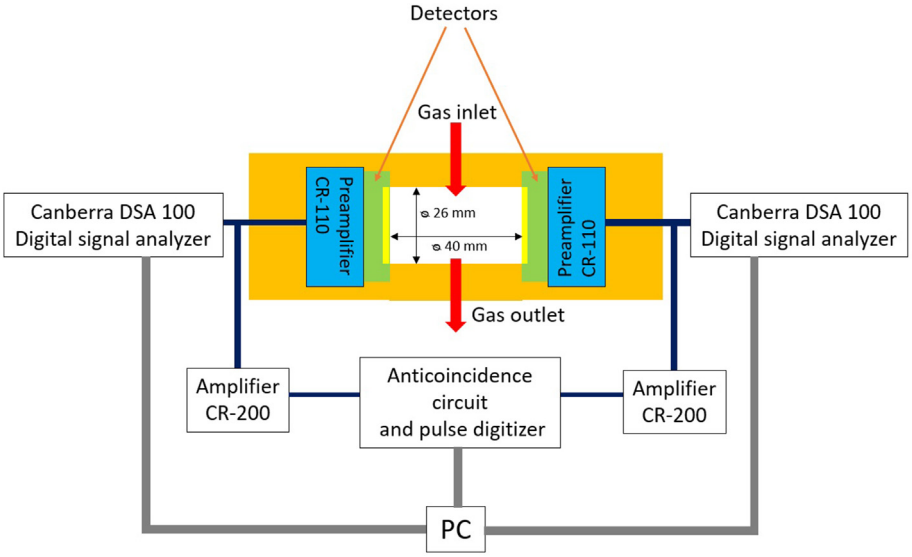

Fig. 3. β-particle detection system.

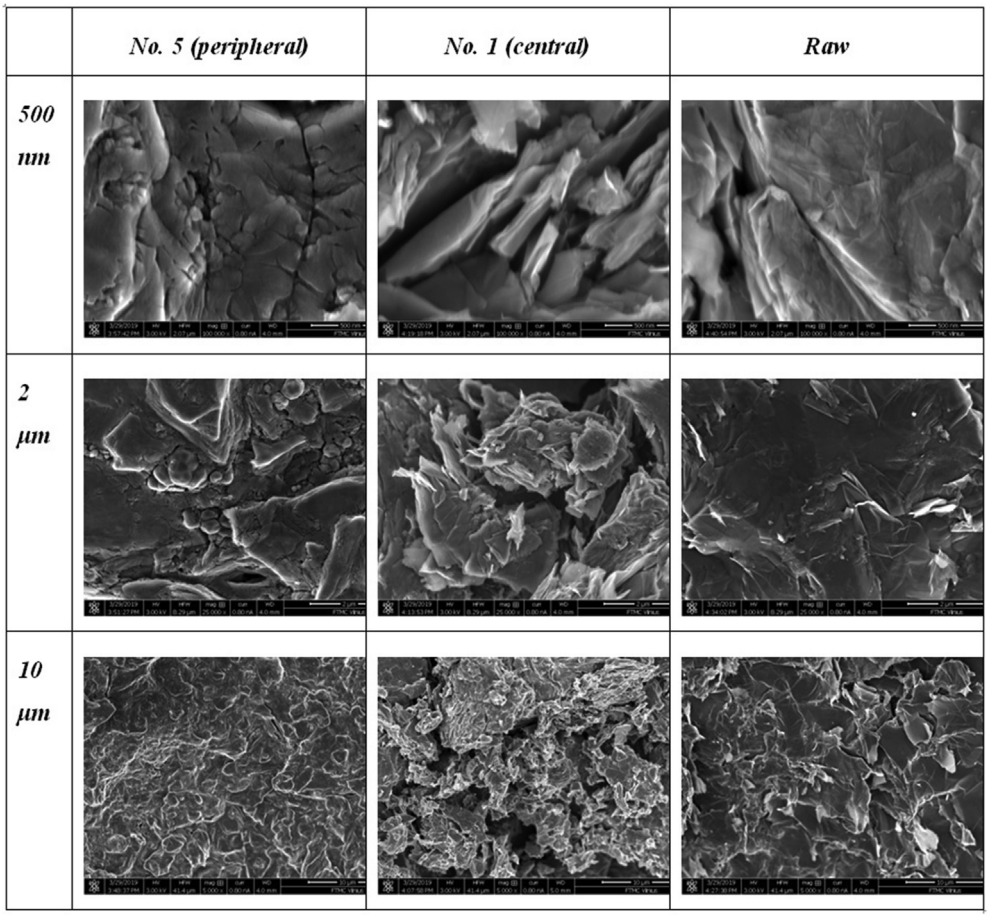

Fig. 4. The SEM images of graphite samples obtained from peripheral and central sites of RBMK-1500 reactor as well as raw graphite sample.

materials including irradiated nuclear grade graphite [28,29]. In this work both raw and irradiated RBMK graphite samples were examined to observe the structural changes induced by neutron irradiation during the operational time of the RBMK-1500 reactor. The Raman spectra are compared in Fig. 5.

The raw graphite sample with cleaved surface without any additional pre-treatment was measured prior to examination of the irradiated graphite samples. The Raman spectrum of the raw graphite sample shows the characteristic G band at around 1580 cm^{-1} as well as small defect induced D peak near 1350 cm^{-1} which appears due to natural non-uniformity of the cleaved surface of graphite sample. The shoulder at 1620 cm^{-1} is known as D′ band and also appears due to the presence of defects. The second-order 2D band is clearly visible at around 2700 cm^{-1}. This band is an overtone of the D band, but, unlike the D band, activation of this mode does not require the presence of the defects [29].

The examination of the irradiated graphite samples shows a significant intensity increase of the defect-induced D band at around 1350 cm^{-1} relative to the symmetry-allowed G band which is found at 1580 cm^{-1}. The D and G bands remain clearly visible, but they become very wide. The intensity of the 2D band at around 2700 cm^{-1} is reduced due to a general rise in intensity at higher wavenumbers. These changes occur due to the radiation induced formation of polycrystalline carbon consisting of small crystallites [30]. Recently, Raman spectroscopic analysis of irradiated Oldbury reactor Pile Grade A (PGA) graphite was carried out by Payne et al. [28]. The Raman spectrum from raw PGA shows the G, D and 2D bands with the G band being dominant. However, a significant increase in the width of both the D and G peaks was also observed in the Raman spectra of irradiated PGA graphite surface. The 2D band also is broadening and decrease in intensity or it is even not present. In general, the profiles of Raman spectra of irradiated RBMK-1500 reactor graphite samples are similar to those obtained in case of examination of the Oldbury reactor graphite samples by Payne et al. [28].

3.2. Evaluation of primary displacement damage

The theoretically evaluated neutron induced primary displacement rates are shown in Table 1. The average DPA per year is evaluated by taking into consideration the constant neutron flux and multiplying the average displacement per atom rate (DPA/s averaged over all calculation methods) by the number of seconds in a year. Our previous evaluations of the DPA rates have shown, that with the 1.36×10^{14} cm^{-2} neutron flux, the average number of DPA per year in graphite stack is around 0.51, with the maximum value of 0.76 DPA per year near the fuel channels, and around 0.38 DPA per year in the graphite column corners [6]. Only the single graphite column with reflective surfaces was simulated in our previous research, while in this research, a whole reactor model was simulated with the neutron flux evaluation at the sample locations in the model. In the 3D RBMK-1500 reactor model, the total neutron flux as well as its energy distribution varies at the different sample locations. Because of this, the DPA rate values obtained differ between one another and between the average value obtained from our previous research. However, the values obtained in

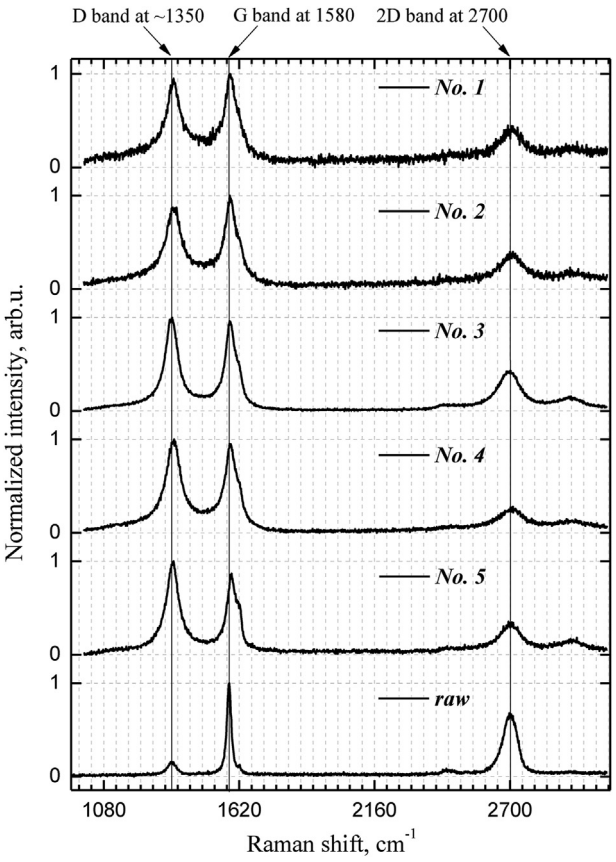

Fig. 5. The Raman spectra of graphite samples obtained from different locations of RBMK-1500 reactor core. The excitation wavelength is 532 nm (0.3 mW).

this research coincide well with the values obtained in previous research. As can be seen in Table 1, only the DPA rate evaluated for the sample ***No.5*** is smaller than the average one, while the DPA of samples ***No.1*** and ***No.4*** are higher due to higher neutron flux or larger fraction of high energy neutrons. Sample ***No.5*** lies in the peripheral zone, and the total neutron fluence is lower than in the central and plateau regions, so the DPA rate is lower.

The values presented in Table 1 are preliminary as the history of the experimental neutron flux in these locations is not well known. The changes in DPA rate could be seen experimentally in the Raman spectra of the samples. The D band of Raman spectrum of sample ***No.2*** (see Fig. 4) appears with lower intensity than the G band; this could indicate a lower displacement damage. However, if the Raman spectrum of the sample ***No.5*** would be taken into consideration, the D band is not smaller than the G band, which means that the theoretical displacement rate is not always accurately observed from the experimental results. It is well known fact, that most of the primary displacement damage is annealed due to the thermal heating [31,32]. Different form of Raman spectrum of sample ***No.5*** could be due to the lower temperature and less effective annealing of defects. This means that although the temperature might be sufficient to anneal the primary defects so they wouldn't agglomerate into amorphous structures, the temperature might be lower than in the central regions so the ratio of survived point and higher order defects could be higher when compared to the samples in the central region of the RBMK-1500 reactor core.

3.3. γ-emitters in the irradiated RBMK-1500 reactor graphite

After structural analysis by both SEM and Raman spectroscopy, the irradiated graphite samples were prepared for $\delta^{13}C$ and ^{14}C measurements. For this purpose initial samples were divided and small parts of them were taken. Radionuclides, which usually are found in the spent nuclear graphite, fall in different groups according to the origin (e.g. impurities, fission products, etc.) as well as distribution in graphite matrix. In order to evaluate the presence of γ-ray emitters in the irradiated RBMK-1500 reactor graphite samples, the γ-spectrometric analysis was performed. Experimentally determined activity of γ-ray emitters in these samples is presented in Table 2.

^{60}Co is one of the main γ-emitters in the irradiated RBMK-1500 reactor graphite. The specific activity of ^{60}Co falls in the range from 331 ± 27 Bq/g to 39500 ± 3160 Bq/g in the measured samples. The highest value of specific ^{60}Co activity is registered in the sample ***No.1*** from the central zone, while the lowest one is obtained in the sample ***No.5*** from the peripheral zone. However, the activity values are very different even in the parts of the same sample. Under reactor operational conditions ^{60}Co is produced mainly due to activation of impurities by the $^{59}Co(n,\gamma)^{60}Co$ reaction. As ^{59}Co impurity is distributed non-uniformly in the nuclear graphite, the contamination by ^{60}Co is also non-homogeneous [33]. ^{60}Co with half-life of 5.3 years is at negligible concentrations after 100 years, so for the long term storage and disposal requirements of the spent nuclear graphite, the radionuclides with half-lives of thousands of years are under concern [34].

^{137}Cs is also detected in every examined sample of irradiated RBMK-1500 reactor graphite. The highest activity value of 1370 ± 83 Bq/g is registered in the sample ***No.3***, while the lowest one of 61 ± 5 Bq/g is obtained when measuring the sample ***No.5***. However, unlike in case of ^{60}Co, the activity differences in the parts of the same sample are not so significant. ^{137}Cs is a fission product. Fission products appear from uranium impurity in the graphite matrix or from the uranium traces from the outer surface of the fuel elements via surface contamination pathway. Both ^{60}Co and ^{137}Cs activity values may be used in the scaling factor method for the determination of activity of other radionuclides in the spent nuclear graphite [35], but only if sufficient number of statistical measurement runs is performed and the averaged values of the

Table 1
Numerically evaluated displacement per atom per second (DPA/s) rates in for different samples based on their location in the reactor. The average DPA/year is obtained by averaging the DPA/s rates over all methods and multiplying by the number of seconds in a year.

Evaluation method	Displacement per atom rate (DPA/s)				
	Sample No.				
	No.1	No.2	No.3	No.4	No.5
NJOY HEATR	3.83×10^{-8}	1.11×10^{-8}	0.93×10^{-8}	3.31×10^{-8}	0.34×10^{-8}
GEANT4	4.01×10^{-8}	1.19×10^{-8}	0.98×10^{-8}	3.46×10^{-8}	0.35×10^{-8}
SPECTRA-PKA ENDF8	4.21×10^{-8}	1.25×10^{-8}	1.03×10^{-8}	3.64×10^{-8}	0.37×10^{-8}
SPECTRA-PKA TENDL	4.16×10^{-8}	1.23×10^{-8}	1.01×10^{-8}	3.60×10^{-8}	0.37×10^{-8}
Average DPA/year	1.28	0.37	0.32	1.10	0.11

Table 2
Experimentally determined activity of γ-ray emitters in graphite samples, Bq/g (k = 1), 2018-01-01. The samples noted as ***No.1***, ***No.2***, etc. refers to the initial samples used for the structural analysis, the samples used for stable carbon isotope ratio ($\delta^{13}C$) measurements are noted as ***No.1a***, ***No.2a***, etc., while ones used for ^{14}C analysis as ***No.1b***, ***No.2b***, etc.

Sample No.	Sample mass, g	Co-60 A, Bq/g	Ba-133 A, Bq/g	Cs-134 A, Bq/g	Cs-137 A, Bq/g	Eu-152 A, Bq/g	Eu-154 A, Bq/g	Eu-155 A, Bq/g
No.1	0.02245	12970 ± 778	153 ± 14	40 ± 4	321 ± 20	<7.3	83 ± 8	100 ± 7
No.1b	0.00019	39500 ± 3160	363 ± 44		257 ± 24		–	70 ± 10
No.1a	0.000074	2100 ± 168	165 ± 21		145 ± 18		–	–
No.2	0.02333	10830 ± 650	<3.0	10 ± 2	96 ± 7	<6.7	<2.4	<4.4
No.2b	0.000422	4900 ± 392	–		66 ± 6		–	–
No.2a	0.0001	4560 ± 365	–		73 ± 10		–	–
No.3	0.0251	12540 ± 752	75 ± 7	35 ± 4	1060 ± 64	<6.1	167 ± 15	173 ± 11
No.3a	0.000278	21700 ± 1740	112 ± 15		987 ± 60		354 ± 58	111 ± 11
No.3b	0.00038	33500 ± 2680	341 ± 42		1370 ± 83		517 ± 58	393 ± 25
No.4	0.01869	1351 ± 82	<1.5	<2.5	66 ± 4	<3,1	<1.4	<2.5
No.4a	0.000152	4310 ± 345	–		139 ± 16		–	–
No.4b	0.000204	2100 ± 168	–		70 ± 7		–	–
No.5	0.02041	4010 ± 241	13 ± 2	17 ± 2	91 ± 6	<4.5	78 ± 7	80 ± 5
No.5b	0.000414	4240 ± 340	–		61 ± 5		–	–
No.5a	0.000272	331 ± 27	–		102 ± 8		–	–

measured nuclide with its confident intervals are estimated. The results of γ measurements carried out in this work imply that ^{60}Co as well as ^{137}Cs distribution in the irradiated RBMK-1500 reactor graphite is not homogeneous and it does not correlate with ^{14}C distribution. The more detailed analysis on nuclide distribution in the RBMK-1500 reactor graphite is presented in [36].

^{134}Cs is produced in the reactor graphite through the activation of ^{133}Cs impurity as well as a fission product [33]. The highest ^{134}Cs activity of 40 ± 4 Bq/g is detected in the sample ***No.1***, while in the sample ***No.4*** it is found below detection limit. Similar data are obtained for ^{133}Ba, however, contrary to ^{134}Cs, its activity is found to be below the detection limit also in the sample ***No.2***. ^{154}Eu and ^{155}Eu, which both are fission products, are detected just in the samples ***No.1***, ***No.3*** and ***No.5***. The activity of ^{152}Eu is found below detection limit in all measured samples.

3.4. Modeling of neutron flux and ^{14}C activity in the RBMK-1500 graphite

In order to assess the real irradiation parameters of the examined RBMK-1500 graphite, the method based on coupling of stable isotope ratio mass spectrometry and MCNP6 modeling is used. Stable carbon isotope ratio ($\delta^{13}C$) measurements in irradiated graphite were described previously as experimental method to evaluate the total neutron flux [13,21]. MCNP6 modeling of the activation of graphite samples in RBMK-1500 neutron flux is performed taking into account the axial and radial power distribution as described above.

In the reactor operational conditions the $^{12}C(n,\gamma)^{13}C$ reaction occurs 3.7 times faster than $^{13}C(n,\gamma)^{14}C$ reaction. This leads to the enhanced accumulation of ^{13}C compared to ^{14}C in irradiated graphite matrix for the certain period of time (21 year of INPP Unit 1 operation). Thus, according to the calculated $\delta^{13}C$ value it is possible to obtain the real neutron flux to which graphite sample was exposed. Both the $\delta^{13}C$ experimental values and the neutron flux recalculated according to $\delta^{13}C$ experimental values are presented in Table 3. The neutron flux calculated at the different sample positions by using 3D MCNP6 model was adjusted to real axial/radial power and corresponding theoretic $\delta^{13}C$ values are also reported in Table 3.

In general, experimentally determined $\delta^{13}C$ values fall in the range from −20.0 to −25.6 in irradiated graphite samples, while in raw graphite sample $\delta^{13}C$ value is equal to −30.7. In the sample from the central zone of the reactor the $\delta^{13}C$ value of −24.5 was obtained, while in graphite samples from the central plateau zone of the reactor it differs from −20.0 to −24.4. In the sample from peripheral zone the $\delta^{13}C$ value of −24.1 was found. In summary, the results indicate clear difference between the irradiated and non-irradiated raw graphite samples. However, the dependence of $\delta^{13}C$ value on the irradiated graphite sample location in reactor core is not found. This indicates that the neutron flux is quite uniform in the RBMK-1500 reactor core. The measured $\delta^{13}C$ values in graphite at different positions of the reactor core indicate that the neutron flux in the samples varies from 7.3×10^{13} n/cm^{2}s to 1.5×10^{14} n/cm^{2}s. Comparing with the modeled neutron flux adjusted to the real axial/radial power and $\delta^{13}C$ – in ***No.1a***, ***No.2a*** and ***No.5a*** samples the differences are in the range of 3–9 % except for samples ***No.3a*** and ***No.4a*** where higher differences of 15–30 % were observed most probably due to sample position in the reactor core (taking into account, that these two samples were taken from the stack graphite of the same fuel channel, but at different height). Actually this allows us to validate 3D MCNP6 model to assess the real irradiation parameters at any place of the RBMK-1500 graphite core within 10 % uncertainty range in all graphite constructions by using this method.

By using the full scale MCNP6 3D model of RBMK-1500 reactor core the realistic neutron flux at each irradiated graphite sample position of RBMK-1500 reactor core was obtained. The modeling results of ^{14}C activity and neutron flux in the RBMK-1500 graphite constructions are given in Table 4.

The flux in the periphery zone differs by 3 times and by order of magnitude in the side reflectors if compared to the plateau region. It can be noted that ^{14}C activity is directly proportional to the neutron fluence value and does not depend on other parameters if there is no additional ^{14}C production due to the inflow of the material (as for example ^{14}N in the cooling gas of the stack). According to the obtained results the production of ^{14}C from ^{14}N in the RBMK-1500 reactor is about ~60 % when using the RBMK-1500 neutron spectrum and 15 ppm of ^{14}N impurity concentration in the graphite matrix.

3.5. Experimental ^{14}C activity determination

For the experimental determination of ^{14}C activity in irradiated graphite samples the rapid analysis method was applied as described previously [12]. In brief, the graphite samples were combusted to CO_2, the evolved CO_2 gas passed to the elemental analyzer for the determination of C (carbon) amount. After that, the CO_2 gas passed to the β-detection system where ^{14}C content was determined. Based on the detected CO_2 amount the total mass of carbon in the sample was determined. The correlation of graphite sample mass as obtained by weighing and by the combustion method is presented in Fig. 6.

Table 3
Experimentally determined as well as modeled $\delta^{13}C$ and corresponding neutron fluxes in the graphite samples.

Sample No.	No.1a	No.2a	No.3a	No.4a	No.5a	Raw
Exp. $\delta^{13}C$	−24.5	−24.4	−25.6	−20.0	−24.1	−30.7
Flux (recalculated according to $\delta^{13}C$), n/cm^{2}s	8.9×10^{13}	9.1×10^{13}	7.3×10^{13}	1.5×10^{14}	9.5×10^{13}	
Flux (model adjusted to real axial/radial power), n/cm^{2}s	9.6×10^{13}	9.4×10^{13}	6.2×10^{13}	1.0×10^{14}	1.0×10^{14}	
Model $\delta^{13}C$	−24.1	−24.2	−26.4	−23.5	−23.5	

Table 4
The results of modeling of neutron flux and ^{14}C activity in the RBMK-1500 reactor graphite constructions for average power of 2152 MW (for 2018-01-01 date).

Graphite construction	Flux, n/cm^2*s	^{14}C A, Bq/g
Graphite stack (plateau region)	1.0×10^{14}	1.44×10^{5}
Graphite stack top&bottom	1.4×10^{13}	3.24×10^{4}
Graphite sleeve	9.9×10^{13}	1.16×10^{5}
Periphery graphite stack	3.0×10^{13}	4.26×10^{4}
Periphery graphite stack top&bottom	4.1×10^{12}	9.67×10^{3}
Graphite reflector	9.7×10^{12}	2.38×10^{4}
Graphite reflector top& bottom	1.4×10^{12}	3.71×10^{3}
Graphite reflector with cooling channel	1.2×10^{12}	3.26×10^{3}
Graphite reflector with cooling top&bottom	1.8×10^{11}	5.07×10^{2}
Graphite CPS channel	9.0×10^{13}	1.60×10^{5}
Graphite CPS channel top& bottom	1.2×10^{13}	2.81×10^{4}

After application of linear approximation it is found that all the samples fall in the 95 % confidence band and the correlation coefficient is ~0.99. These results are in good agreement with previous research were correlation between these two independent methods was found with the correlation coefficient of about 0.97 [12].

During the sample combustion process the CO_2 gas flows through the detection chamber where β-activity pulses are detected (Fig. 7). Usually 2–3 combustion cycles are needed to burn-down the graphite sample completely. The number of cycles needed depends not only on the mass of the graphite sample and its porosity but also on the amount of the oxidation agent. No CO_2 signal from TCD ensures that graphite combustion process is completed.

The combined data from TCD as well as from β detection system are presented in Fig. 8. The β-counts start to increase at about 300–400 s during the sample combustion cycle with a slight delay compared to the increase of the TCD signal. This occurs due to the geometrical characteristics of the β-detection system i.e. the volume of the β detection chamber is larger compared to one of the gas tubes.

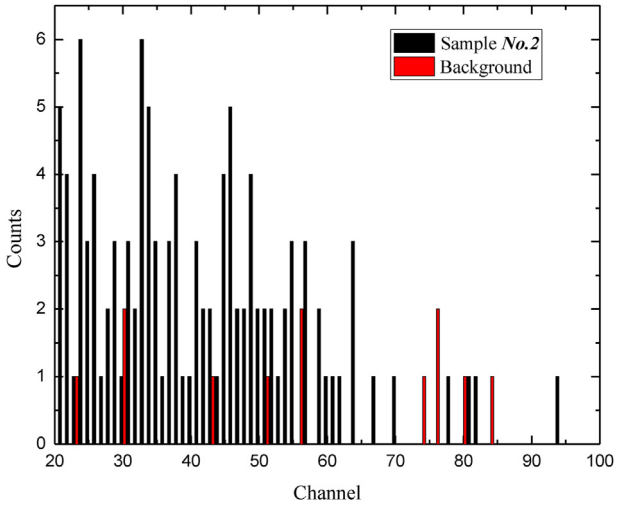

Fig. 7. The spectrum of ^{14}C in the graphite sample ***No.2*** registered by semiconductor detector.

Based on the sum of the β-pulses encountered during all combustion cycles the total sample activity is evaluated. In the case of LSC measurements, the gas catchers are not changed until the combustion of the sample is complete. It means that the total amount of the CO_2 from the whole graphite sample is collected in the alkaline solution to represent the total activity of the given sample.

The comparison of the data obtained by both semiconductor detector and LSC method is presented in Fig. 9. It is observed that data from these two independent methods exhibit a linear

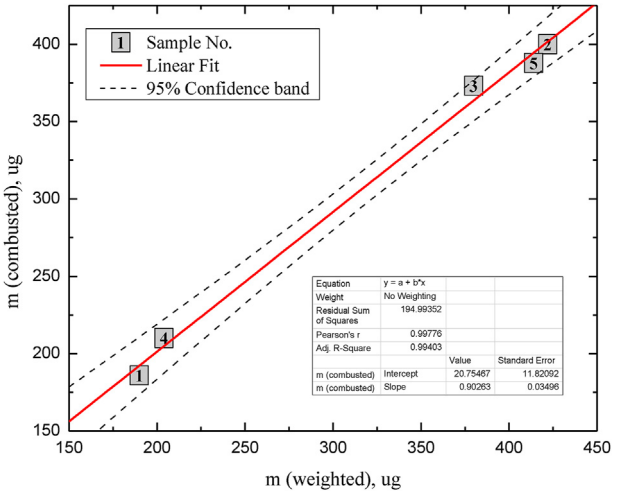

Fig. 6. The correlation of graphite sample mass obtained independently by weighing as well as by the CO_2 mass after combustion in the elemental analyzer system. The Adj. R-Square value of the linear approximation is 0.99.

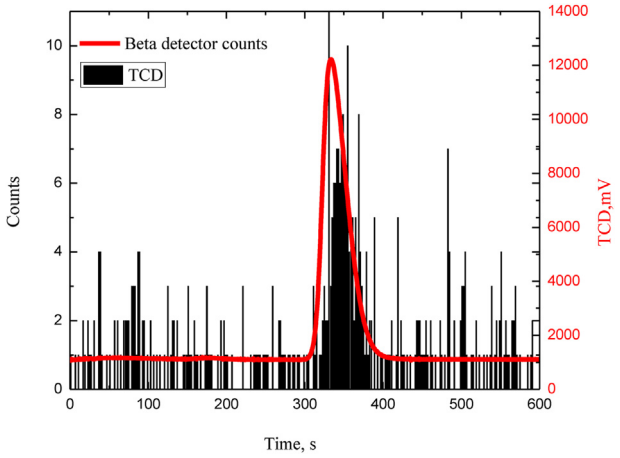

Fig. 8. The TCD signal indicating intensity of CO2 flow and β counts registered by semiconductor detector during the combustion of the graphite sample No.2.

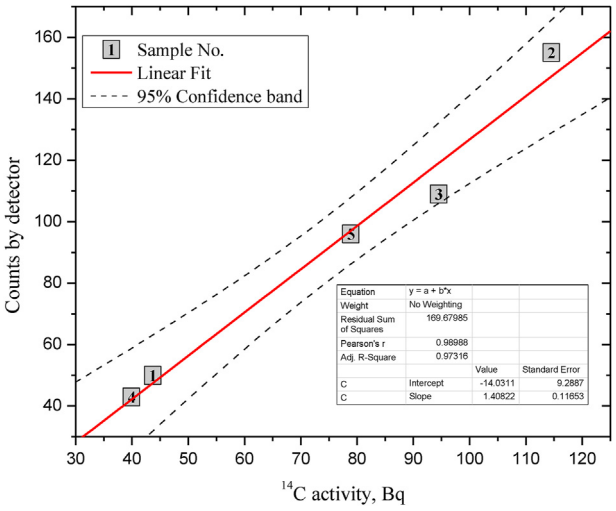

Fig. 9. The correlation of ^{14}C activity in graphite samples obtained independently by LSC as well as by β detector. The Adj. R-Square value of the linear approximation is 0.97.

Table 5
Experimentally determined mass of graphite samples as well as ^{14}C activity.

Sample No.	Sample mass, μg		^{14}C activity, Bq	^{14}C activity, Bq/g
	By weighing	By CO_2 amount		
No.1b	190	186	43.7 ± 2.5	(2.30 ± 0.13) × 10^5
No.2b	422	400	114.5 ± 6.5	(2.71 ± 0.16) × 10^5
No.3b	380	373	94.5 ± 5.5	(2.49 ± 0.14) × 10^5
No.4b	204	210	39.9 ± 2.3	(1.96 ± 0.11) × 10^5
No.5b	414	388	78.9 ± 4.6	(1.91 ± 0.11) × 10^5

dependence with a correlation coefficient of ~0.99, while all values fall in the 95 % confidence band. Comparing with results obtained previously (R = 0.94) [12], one can find out that the current version of the experimental setup is more precise.

The experimentally measured ^{14}C activity in the graphite samples is by ~1.5 times higher compared to modeling in the graphite stack (see Tables 4 and 5 for details). This could be due to the higher production of ^{14}C from ^{14}N in the RBMK-1500 reactor. ^{14}N impurity concentration of 15 ± 4 ppm was used for modeling in graphite activation based on previous RBMK-1500 reactor graphite activation measurements [13]. However, the ^{14}N impurity concentration of 25–35 ppm corresponds to measured activities of samples of RBMK-1500 reactor graphite.

4. Conclusions

The structural and radiological characterization of irradiated RBMK-1500 reactor graphite is important for the radioactive graphite waste management. Structural properties of the irradiated graphite influence behavior of radionuclides in the graphite matrix under disposal conditions. Radiological characterization of the irradiated nuclear graphite aims to identify major contributors to radioactive contamination of the spent nuclear graphite waste. In this study the following observations are reported:

- Irradiated RBMK-1500 reactor graphite exhibits significant reduction in crystallites size when compared to the raw RBMK graphite. However, amorphous fraction is very low in both samples from the central and peripheral zone of the RBMK-1500 reactor core.
- Numerically evaluated displacement per atom per year values vary from 1.28 DPA/year in the central region to 0.11 DPA/year in the peripheral zone of the RBMK-1500 reactor core.
- Distribution of γ-ray emitters is non-homogeneous in the irradiated RBMK-1500 reactor graphite matrix; the main γ-ray emitters are ^{60}Co and ^{137}Cs. The number of samples is not sufficient for scaling factor determination between ^{60}Co and other nuclides.
- The measured δ^{13}C values indicate that the neutron flux in the samples from different positions varies from 7.3 × 10^{13} n/cm^{2}s to 1.5 × 10^{14} n/cm^{2}s. The neutron flux is quite uniform in the entire RBMK-1500 reactor core (no dependence of δ^{13}C value was found when comparing plateau and peripheral regions).
- Measured ^{14}C specific activity values in the irradiated RBMK-1500 reactor graphite samples vary from 190 kBq/g to 270 kBq/g. This corresponds to 25–35 ppm ^{14}N impurity concentration.

It should be noted that observations presented in this study are obtained by examination of five samples only which were taken from the different positions of RBMK-1500 reactor core. Therefore, the results may not be representative when characterizing the total amount of irradiated graphite from the whole RBMK-1500 reactor core. When interpreting results of activity of γ emitters the possibility of random distribution of the traces of uranium products on the graphite surfaces directly exposed to the fuel channel needs to be accounted for. Also, it should be noted, that the real irradiation history is unknown for the particular sample and this may lead to mismatch when comparing the experimentally obtained δ^{13}C values and calculated ones. However, the brief results of structural analysis obtained in this study are important for further detailed structural research of irradiated RBMK-1500 reactor graphite. Furthermore, some observations described here e.g. ^{14}C activity are in good agreement with previous studies. Moreover, the improved version of the previously reported rapid analysis method showed more precise results than it was obtained before. Thus, study described here could be useful for further analysis of irradiated RBMK-1500 graphite (e.g. ^{14}C spatial distribution inside the first few millimeters of the graphite surface) as well as graphite of other graphite-moderated reactors.

Declaration of competing interest

The authors declare that they have no known competing financial interests or personal relationships that could have appeared to influence the work reported in this paper.

Acknowledgements

We would like to acknowledge Dr. Giedrius Stalnionis from Department of Characterization of Materials Structure (Center for Physical Sciences and Technology, Lithuania), who helped us to obtain high quality SEM images of both irradiated and raw graphite samples.

References

[1] Galutinis Ignalinos AE Eksploatavimo Nutraukimo Planas: Atliekų Tvarkymas, 2018.
[2] K. Almenas, A. Kaliatka, E. Uspuras, Ignalina RBMK-1500 A Source Book, Lithuanian Energy Institute, 1998.
[3] E. Narkunas, P. Poskas, A. Smaizys, S. Norris, Estimation of the inventory of 14 C and other key radionuclides in irradiated RBMK-1500 graphite based on limited measurements and full 3D core modeling, Radiocarbon 60 (2018) 1849–1859, https://doi.org/10.1017/RDC.2018.122.
[4] M.D. Bondar'kov, D.M. Bondar'kov, A.M. Maksimenko, V.A. Zheltonozhskii, M.V. Zheltonozhskaya, V.V. Petrov, A.I. Savin, Activity study of graphite from

the chernobyl NPP reactor, Bull. Russ. Acad. Sci. Phys. 73 (2009) 261–265, https://doi.org/10.3103/S1062873809020300.
[5] IAEA-TECDOC-1154, Irradiation Damage in Graphite Due to Fast Neutrons in Fission and Fusion Systems, 7, IAEA, 2000.
[6] D. Lingis, E. Lagzdina, A. Plukis, R. Plukienė, V. Remeikis, Evaluation of the primary displacement damage in the neutron irradiated RBMK-1500 graphite, Nucl. Instrum. Methods Phys. Res. Sect. B Beam Interact. Mater. Atoms 436 (2018) 9–17, https://doi.org/10.1016/j.nimb.2018.08.038.
[7] B. Zlobenko, B. Shabalin, V. Skripkin, Y. Fedorenko, V. Yatzenko, Report on graphite categories in the RBMK reactor (D5.3) Version 2, CArbon-14 Source Term CAST Project (2016) 1–28.
[8] T.D. Burchell, P.J. Pappano, J.P. Strizak, A study of the annealing behavior of neutron irradiated graphite, Carbon N. Y. 49 (2011) 3–10, https://doi.org/10.1016/j.carbon.2010.08.026.
[9] Valstybės Įmonė Ignalinos Atominė Elektrinė, Ignalinos Atominės Elektrinės Galutinis Eksploatavimo Nutraukimo Planas, 2020.
[10] IAEA, Treatment of irradiated graphite to meet acceptance criteria for waste disposal, ACTIVE (2010) T21026. https://www.iae.lt/veikla/eksploatavimo-nutraukimas/dalyvavimas-sprendimu-priemime/307.
[11] M.E. Pick, Magnox Graphite Core Decommissioning and Disposal Issues, Baseline. ((n.d.)).
[12] V. Remeikis, E. Lagzdina, A. Garbaras, A. Gudelis, J. Garankin, R. Plukienė, L. Juodis, G. Duškesas, D. Lingis, V. Abdulajev, A. Plukis, Rapid analysis method for the determination of 14C specific activity in irradiated graphite, PloS One 13 (2018), https://doi.org/10.1371/journal.pone.0191677.
[13] V. Remeikis, A. Plukis, R. Plukienė, A. Garbaras, R. Barisevičiūtė, A. Gudelis, R. Gvozdaitė, G. Duškesas, L. Juodis, Method based on isotope ratio mass spectrometry for evaluation of carbon activation in the reactor graphite, Nucl. Eng. Des. 240 (2010) 2697–2703, https://doi.org/10.1016/j.nucengdes.2010.06.020.
[14] R. Plukienė, E. Lagzdina, L. Juodis, A. Plukis, A. Puzas, R. Gvozdaitė, V. Remeikis, Z. Révay, J. Kučera, D. Ancius, D. Ridikas, Investigation of impurities of RBMK graphite by different methods, Radiocarbon 60 (2018) 1861–1870, https://doi.org/10.1017/RDC.2018.93.
[15] R. Macfarlane, D.W. Muir, R.M. Boicourt, A.C. Kahler III, J.L. Conlin, The NJOY Nuclear Data Processing System, Version 2016, Los Alamos, NM (United States), 2017, https://doi.org/10.2172/1338791.
[16] M.R. Gilbert, J. Marian, J.C. Sublet, Energy spectra of primary knock-on atoms under neutron irradiation, J. Nucl. Mater. 467 (2015) 121–134, https://doi.org/10.1016/j.jnucmat.2015.09.023.
[17] M. Herman, ENDF-6 Formats Manual Data Formats and Procedures for the Evaluated Nuclear Data File ENDF/B-VI and, ENDF/B-VII, Upton, NY (United States), 2009, https://doi.org/10.2172/981813.
[18] R.E. MacFarlane, A.C. Kahler, Methods for processing ENDF/B-vii with NJOY, Nucl. Data Sheets 111 (2010) 2739–2890, https://doi.org/10.1016/j.nds.2010.11.001.
[19] M.J. Norgett, M.T. Robinson, I.M. Torrens, A proposed method of calculating displacement dose rates, Nucl. Eng. Des. 33 (1975) 50–54, https://doi.org/10.1016/0029-5493(75)90035-7.
[20] S. Agostinelli, J. Allison, K. Amako, J. Apostolakis, H. Araujo, P. Arce, M. Asai, D. Axen, S. Banerjee, G. Barrand, F. Behner, L. Bellagamba, J. Boudreau, L. Broglia, A. Brunengo, H. Burkhardt, S. Chauvie, J. Chuma, R. Chytracek, G. Cooperman, G. Cosmo, P. Degtyarenko, A. Dell'Acqua, G. Depaola, D. Dietrich, R. Enami, A. Feliciello, C. Ferguson, H. Fesefeldt, G. Folger, F. Foppiano, A. Forti, S. Garelli, S. Giani, R. Giannitrapani, D. Gibin, J.J. Gómez Cadenas, I. González, G. Gracia Abril, G. Greeniaus, W. Greiner, V. Grichine, A. Grossheim, S. Guatelli, P. Gumplinger, R. Hamatsu, K. Hashimoto, H. Hasui, A. Heikkinen, A. Howard, V. Ivanchenko, A. Johnson, F.W. Jones, J. Kallenbach, N. Kanaya, M. Kawabata, Y. Kawabata, M. Kawaguti, S. Kelner, P. Kent, A. Kimura, T. Kodama, R. Kokoulin, M. Kossov, H. Kurashige, E. Lamanna, T. Lampén, V. Lara, V. Lefebure, F. Lei, M. Liendl, W. Lockman, F. Longo, S. Magni, M. Maire, E. Medernach, K. Minamimoto, P. Mora de Freitas, Y. Morita, K. Murakami, M. Nagamatu, R. Nartallo, P. Nieminen, T. Nishimura, K. Ohtsubo, M. Okamura, S. O'Neale, Y. Oohata, K. Paech, J. Perl, A. Pfeiffer, M.G. Pia, F. Ranjard, A. Rybin, S. Sadilov, E. Di Salvo, G. Santin, T. Sasaki, N. Savvas, Y. Sawada, S. Scherer, S. Sei, V. Sirotenko, D. Smith, N. Starkov, H. Stoecker, J. Sulkimo, M. Takahata, S. Tanaka, E. Tcherniaev, E. Safai Tehrani, M. Tropeano, P. Truscott, H. Uno, L. Urban, P. Urban, M. Verderi, A. Walkden, W. Wander, H. Weber, J.P. Wellisch, T. Wenaus, D.C. Williams, D. Wright, T. Yamada, H. Yoshida, D. Zschiesche, Geant4—a simulation toolkit, Nucl. Instruments Methods Phys. Res. Sect. A Accel. Spectrometers, Detect. Assoc. Equip. 506 (2003) 250–303, https://doi.org/10.1016/S0168-9002(03)01368-8.
[21] A. Garbaras, E. Bružas, V. Remeikis, Stable carbon isotope ratio (δ13C) measurement of graphite using EA-IRMS system, Mater. Sci. (2015) 2–7, https://doi.org/10.5755/j01.mm.21.2.6873.
[22] T. Goorley, M. James, T. Booth, F. Brown, J. Bull, L.J. Cox, J. Durkee, J. Elson, M. Fensin, R.A. Forster, J. Hendricks, H.G. Hughes, R. Johns, B. Kiedrowski, S. Mashnik, G. Mckinney, D. Pelowitz, R. Prael, J. Sweezy, L. Waters, T. Zukaitis, G. Mckinney, D. Pelowitz, R. Prael, J. Sweezy, L. Waters, T. Wilcox, T. Zukaitis, Initial MCNP6 Release Overview INITIAL MCNP6 RELEASE OVERVIEW, 2017, p. 5450, https://doi.org/10.13182/NT11-135.
[23] D. Ancius, D. Ridikas, R. Plukiene, Evaluation of the activity of irradiated graphite in the Ignalina nuclear power evaluation of the activity of irradiated graphite in the Ignalina nuclear power plant RBMK-1500 reactor, Nukleonika 50 (2005) 113–120.
[24] R. Plukienė, A. Plukis, A. Puzas, V. Remeikis, Modelling of impurity activation in the RBMK reactor graphite using MCNPX, Prog. Nucl. Sci. Technol. 2 (2011) 421–426, https://doi.org/10.15669/pnst.2.421.
[25] A. Plukis, R. Plukienė, V. Barkauskas, G. Duškesas, D. Germanas, L. Juodis, E. Lagzdina, V. Remeikis, The 3D model for radioactive graphite characterization in the Ignalina NPP RBMK-1500 reactor. Proc., PHYSOR 2018, Cancun, Mex, 2018.
[26] D.A. Brown, M.B. Chadwick, R. Capote, A.C. Kahler, A. Trkov, M.W. Herman, A.A. Sonzogni, Y. Danon, A.D. Carlson, M. Dunn, D.L. Smith, G.M. Hale, G. Arbanas, R. Arcilla, C.R. Bates, B. Beck, B. Becker, F. Brown, R.J. Casperson, J. Conlin, D.E. Cullen, M. Descalle, R. Firestone, T. Gaines, K.H. Guber, A.I. Hawari, J. Holmes, T.D. Johnson, T. Kawano, B.C. Kiedrowski, A.J. Koning, S. Kopecky, L. Leal, Endf/B-viii . 0 : the 8 th major release of the nuclear reaction data library with CIELO-project cross sections , new standards and thermal scattering data, Nucl. Data Sheets 148 (2018) 1–142, https://doi.org/10.1016/j.nds.2018.02.001.
[27] A. Jasiulevičius, Analysis Methodology for RBMK-1500 Core Safety and Investigations on Corium Coolabiblty during a LWR Sever Accidnet, Energiteknik, Stockholm, 2003.
[28] L. Payne, P.J. Heard, T.B. Scott, Examination of surface deposits on Oldbury reactor core graphite to determine the concentration and distribution of 14C, PloS One 11 (2016) 1–19, https://doi.org/10.1371/journal.pone.0164159.
[29] M.A. Pimenta, G. Dresselhaus, M.S. Dresselhaus, L.G. Cançado, A. Jorio, R. Saito, Studying disorder in graphite-based systems by Raman spectroscopy, Phys. Chem. Chem. Phys. 9 (2007) 1276–1291, https://doi.org/10.1039/b613962k.
[30] A.C. Ferrari, J. Robertson, Resonant Raman spectroscopy of disordered, amorphous, and diamondlike carbon, Phys. Rev. B Condens. Matter 64 (2001) 1–13, https://doi.org/10.1103/PhysRevB.64.075414.
[31] E. Lagzdina, D. Lingis, A. Plukis, R. Plukienė, M. Gaspariūnas, I. Matulaitienė, V. Kovalevskij, G. Niaura, V. Remeikis, Structural investigation of RBMK nuclear graphite modified by 12C+ ion implantation and thermal treatment, Nucl. Instrum. Methods Phys. Res. Sect. B Beam Interact. Mater. Atoms 444 (2019) 23–32, https://doi.org/10.1016/j.nimb.2019.01.049.
[32] N. Galy, N. Toulhoat, N. Moncoffre, Y. Pipon, N. Bérerd, M.R. Ammar, P. Simon, D. Deldicque, P. Sainsot, Ion irradiation used as surrogate of neutron irradiation in graphite: consequences on14C and36Cl behavior and structural evolution, J. Nucl. Mater. 502 (2018) 20–29, https://doi.org/10.1016/j.jnucmat.2018.01.058.
[33] V.N. Bushuev, A.V. Verzilov, M. Yu, Zubarev, Radionuclide Characterization of Graphite Stacks from Plutonium Production Reactors of the Siberian Group of Chemical Enterprises, IAEA, 2001.
[34] IAEA-TECDOC-1521, Characterization, Treatment and Conditioning of Radioactive Graphite from Decommissioning of Nuclear Reactors, IAEA, 2006.
[35] IAEA Nuclear Energy Series, Determination and Use of Scaling Factors for Waste Characterization in Nuclear Power Plants, IAEA Tech. Reports, 2009. No. NW-T-1.
[36] V. Remeikis, R. Plukienė, A. Plukis, V. Barkauskas, A. Gudelis, R. Druteikienė, R. Gvozdaitė, L. Juodis, G. Duškesas, E. Lagzdina, D. Germanas, D. Ridikas, S. Krutovcov, Characterisation of RBMK-1500 graphite: a method to identify the neutron activation and surface contamination terms, Nucl. Eng. Des. 361 (2020), https://doi.org/10.1016/j.nucengdes.2019.110501.